ACS Catalysis

Research Article

pubs.acs.org/acscatalysis

Bifunctional Organorhodium Solid Acid Catalysts for Methanol Carbonylation

Lee D. Dingwall,[†,‡] Adam F. Lee,*[,†] Jason M. Lynam,*[,‡] Karen Wilson,*[,†] Luca Olivi,[§] Jon M. S. Deeley,[∥] Sander Gaemers,[∥] and Glenn J. Sunley[∥]

[†]Cardiff Catalysis Institute, School of Chemistry, Cardiff University, Cardiff, CF10 3AT, U.K.

[‡]Department of Chemistry, University of York, York, YO10 5DD, U.K.

[§]Sincrotrone Trieste, Basovizza, Trieste, Italy

[∥]BP Chemicals Limited, Saltend, Hull HU12 8DS, U.K.

Supporting Information

ABSTRACT: Robust, bifunctional catalysts comprising Rh(CO)(Xantphos) exchanged phosphotungstic acids of general formulas $[Rh(CO)(Xantphos)]^{+}_{n}[H_{3-n}PW_{12}O_{40}]^{n-}$ have been synthesized over silica supports which exhibit tunable activity and selectivity toward direct vapor phase methanol carbonylation. The optimal Rh:acid ratio = 0.5, with higher rhodium concentrations increasing the selectivity to methyl acetate over dimethyl ether at the expense of lower acidity and poor activity. On-stream deactivation above 200 °C reflects Rh decomplexation and reduction to Rh metal, in conjunction with catalyst dehydration and loss of solid acidity because of undesired methyl acetate hydrolysis, but can be alleviated by water addition and lower temperature operation.

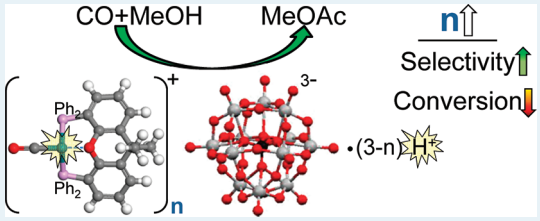

KEYWORDS: *rhodium, heteropoly acid, methanol, carbonylation, EXAFS*

1. INTRODUCTION

Acetic acid is an important industrial chemical, used in paints, plastics, and as a solvent for many important reactions including the formation of many household polymers. As a result of this heavy demand, 12 million tonnes of acetic acid are produced annually, of which 80% of this is produced by methanol (MeOH) carbonylation (Scheme 1).[1] Current industrial processes utilize rhodium (the BP Monsanto process) and iridium (Cativa) catalyzed homogeneous reactions,[2] which can deliver high activity and selectivity but utilize high CO pressures and methyl iodide, liberating highly corrosive HI in situ,[3,4] requiring exotic reactor materials. However, there is considerable interest in the development of alternative, heterogeneous catalyst technologies able to activate both methanol and CO,[4−6] and promote carbonylation over the competing condensation or dehydration pathways shown in Scheme 1. Solid catalysts offer several advantages including simplified product separation, elimination of corrosive halide promoters (and thus mild reaction conditions), and the possibility of continuous plug-flow processing and simpler product separation.

Scheme 1. Important Reaction Pathways during Methanol Carbonylation[a]

$$2\,CH_3OH + CO \rightleftharpoons CH_3COOCH_3 + H_2O \quad (1)$$

$$2\,CH_3OH \rightleftharpoons CH_3OCH_3 + H_2O \quad (2)$$

$$CH_3OCH_3 + CO \rightleftharpoons CH_3COOCH_3 \quad (3)$$

$$2\,CH_3OH \rightleftharpoons C_2H_4 + 2H_2O \quad (4)$$

$$2\,CH_3OH + H_2 \rightleftharpoons C_2H_6 + 2H_2O \quad (5)$$

[a](1) Direct methanol carbonylation to methyl acetate, (2) methanol condensation to dimethyl ether (DME), (3) direct DME carbonylation to methyl acetate, (4) methanol dehydration to higher alkenes, (5) methanol reduction to higher alkanes (MTG chemistry).

Several strategies for heterogeneous carbonylation to acetic acid have been devised, including direct syngas conversion thereby bypassing the need for preliminary methanol production. Unfortunately, syngas to acetyls processes favor hydrocarbon and polymeric products (leading to catalyst coking), yielding little oxygenates. Rhodium-based catalysts are the most effective for the syngas route because of their unique selectivity toward C_2 oxygenates,[7,8] and are usually doped with alkali or transition metals (e.g., Sc, Mn, Ir, Ti) to improve selectivity and/or conversion.[9−11] Selectivities >65% to acetic acid have been achieved over Rh−Mn−Ir−Li/SiO_2, albeit using a CO enriched syngas feed. Another problem with the syngas approach is the facile reduction of many rhodium complexes at temperatures as low as 120 °C under hydrogen atmospheres.[12] While non-rhodium, iodide-free systems are attractive because of lower costs, few have been successfully developed, although Ru−Sn catalysts can generate C_2 oxygen-

Received: January 24, 2012
Revised: May 17, 2012
Published: May 17, 2012

   dx.doi.org/10.1021/cs3000528 | ACS Catal. 2012, 2, 1368−1376

ates from a MeOH-only feed via dehydrogenation to methyl formate followed by isomerization to acetic acid.[13] However, these bimetallic catalysts suffer low conversions (~5%) and methyl formate selectivity (~60%), hence the prevalence of commercial direct methanol carbonylation processes.

Metal loaded mordenites are capable of carbonylating methanol;[14−17] however, little non-iodide work has been undertaken on these systems. Cu mordenite exhibits acetyl selectivities >70% under forcing conditions (350 °C and 25 bar), but undergoes methanol to gasoline (MTG) chemistry before forming acetyls and also deactivates on-stream. In an interesting variation, Cu mordenite was recently combined with Pd/CeO_2 to enable in situ CO generation and thus subsequent carbonylation using a MeOH-only reactor feed, though with comparatively low space time yields.[18] Other solid acid catalysts, such as heteropoly acids (HPAs), have shown promise for the vapor phase carbonylation of methanol[4,19] or dimethyl ether[20] when combined with rhodium via simple ion-exchange.[21] HPAs are polyoxometalate inorganic cage structures, which may adopt the Keggin form with the general formula $H_{3(or\ 4)}MX_{12}O_{40}$, where M is typically P or Si, and X is usually W or Mo. They have been widely studied as catalytic materials because of their tunable (strong) acidity and redox capacity.[22−24] Phosphotungstic acid, $H_3PW_{12}O_{40}.6H_2O$, is one of the most acidic and stable of the Keggin HPAs,[25] whose acidity originates from $H_5O_2^+$ crystallized between Keggin units. This water of crystallization can be ion-exchanged with other cations, for example, Na^+, K^+, Cs^+, or Ag^+, to regulate HPA solubility or acid strength, or exchanged with a catalytically active component to facilitate bifunctional catalysis. A characteristic of their superacidity is the facility for low temperature alkane and alcohol activation, the latter representing a key step in methanol carbonylation.[26] Despite their versatility, HPAs have a poor affinity for CO, and are hence inactive for continuous carbonylation when used alone. Their bulky nature and distributed charge does offer a solution to this problem however, since HPAs can be considered as analogous to other counter-anions, for example, BF_4^- species which can stabilize cationic organorhodium complexes themselves known to reversibly bind CO (and active in alkene hydroformylation).[27,28] An important aspect of the latter Rh(I) complexes is their good thermal and chemical tolerance, imparted through coordination to Xantphos, a polydentate, organophosphorous heterocyclic ligand with a wide bite angle. RhXantphos complexes have shown recent promise in the homogeneous carbonylation of methanol to acetic acid under high CO pressures.[29−31] Here we build upon initial discoveries made in the laboratories of BP Chemicals Limited on the efficacy of bifunctional HPA metal complex based catalysts for methanol carbonylation to explore whether the CO capture properties of such robust RhXantphos cations can be combined with the solid acidity of $H_3PW_{12}O_{40}$ to create a new bifunctional catalyst capable of low temperature, heterogeneous methanol carbonylation.

2. EXPERIMENTAL SECTION

2.1. Catalyst Preparation. Syntheses were performed under a nitrogen or argon atmosphere using standard Schlenk and glovebox techniques. THF and hexane were purified with an Innovative Technologies anhydrous solvent engineering system. $Rh(\kappa^2O\text{-acac})(CO)_2$ and Xantphos were obtained from Aldrich and used as supplied.

a. $Rh(\kappa^2O\text{-acac})(CO)(Xantphos)$ - RhX. RhX was prepared adapting published methods.[27,31] Briefly, 53 mg of $Rh(\kappa^2O\text{-acac})(CO)_2$ (0.211 mmol) and 119.5 mg of Xantphos (0.212 mmol) were added to a Schlenk tube with a stirrer bar and degassed. Upon THF addition (6 mL) the resulting solution turned a red-brown color accompanied by CO evolution, which was removed under vacuum to force the reaction to completion and the solution stirred for a further 15 min. Solvent removal in vacuo and washing with hexane gave 153.6 mg of a yellow/brown powder (90.1% nominal yield RhX): Supporting Information, Figures S1 and S2a $^{31}P\{^1H\}$ NMR (C_6D_6) δ = 11.0 (d, 90.2 Hz $^1J_{Rh-P}$); ν_{CO} = 1974 cm^{-1}; elemental analysis for $C_{45}H_{39}O_4P_2Rh$ expected (mass %) = C (66.84), H (4.86), O (7.91), P (7.66), Rh (12.73), actual (mass %) = C (68.70), H (4.96), P (6.33), Rh (12.06).

b. $[Rh(CO)(Xantphos)][H_3PW_{12}O_{40}.20H_2O]$ - RhXHPW. RhXHPW was synthesized with a 1:1 Rh:HPW ratio as follows. In a separate round-bottom flask 1.246 g of HPW (0.39 mmol) was stirred in 10 mL of degassed tetrahydrofuran (THF). The HPW solution was added to a Schlenk tube containing the required amount of RhX and stirred for a further 15 min. The solvent was removed in vacuo, and the resulting brown powder washed with hexane by canula filtration. A typical yield of 1.12 g (80 mol %) was obtained for the 1:1 Rh:HPW material: Supporting Information, Figures S2b, S3, and S4a-b. ^1H NMR (d_6-DMSO) 6.8−8.2 (m), $^{31}P\{^1H\}$ δ = 44.97 (bs, Rh−P), 14.97 (s, HPW); ν_{CO} = 2008 cm^{-1}; elemental analysis for $C_{40}H_{34}O_{42}P_3RhW_{12}$ expected (mass %) = C (13.00), H (1.25), O (20.77), P (2.51), Rh (2.78), W (59.68), actual (mass%) = C (15.59), H (1.97), P (2.56), Rh (2.64), W (56.27).

c. $RhXHPW/SiO_2$. A series of silica supported variants of RhXHPW were prepared with nominal Rh:HPW ratios of 0.5:1, 1:1, 2:1, and 3:1. In a round-bottom flask, 1.246 g of HPW (0.39 mmol) and 1.099 g of Davisil 100 silica were stirred in 10 mL of degassed THF for 3 h. After impregnation of the HPW on to silica to give 50 wt % HPW/SiO_2, which results in a monolayer dispersion,[32,33] the required amount of RhX solution (5 mL of 0.038 M for 1:1 Rh:W) was added to give the desired Rh:HPW ratio, and the solution stirred for a further 15 min. Solvent was removed by rotary evaporator, and the remaining brown powder dried overnight at 60 °C in a vacuum oven. A typical yield of 2.47 g (98 mass%) was obtained for the 1:1 Rh:HPW/SiO_2 material.

2.2. Catalyst Characterization. Elemental analysis was performed by MEDAC. Rh and W loadings were determined using a Varian Vista MPX ICP-OES, and chlorine analysis via Schöniger flask combustion followed by titration or ion-chromatography. CHN utilized CE-440 and Carlo Erba elemental analysers. A Jeol ECX400 400 MHz NMR spectrometer was used for solution state ^1H and ^{31}P measurement; samples were prepared in d_6-DMSO, and the relaxation time set to 7.5 ms because of the slow relaxation of phosphorus in HPW. A Bruker Daltronics micrOTOF mass spectrometer was used for ESI-MS analysis of positive and negative ion fragments resulting from dissolution of Rh compounds in CH_3CN.

Thermogravimetric analysis (TGA) and Differential Thermal Analysis (DTA) were performed on a Stanton Redcroft STA-780 series thermal analyzer. Samples were heated in an alumina crucible to 1000 °C under 20 mL/min He at 20 °C min^{-1}. Nitrogen porosimetry was performed on a Nova-1200 gas sorption analyzer, applying the Brunauer−Emmett−Teller (BET) isotherm to determine surface areas and the Barrett−

dx.doi.org/10.1021/cs3000528 | ACS Catal. 2012, 2, 1368−1376

Joyner−Halenda approximation to calculate pore radius and volume. DRIFTS was performed on a Thermo Nicolet Avator 370 MCT with smart collector accessory, using a water-cooled environmental chamber with ZnSe window. Temperature programmed pyridine desorption experiments were performed by addition of 2 cm^3 neat pyridine to 100 mg of catalyst, followed by drying at room temperature. Samples were diluted with KBr powder (2 wt %), then loaded into the chamber and evacuated at 70 °C prior to measurement. Samples analysis utilized the Kubelka−Munk approximation to quantify peak areas.

X-ray photoelectron spectroscopy (XPS) was performed on a Kratos AXIS HSi instrument equipped with a charge neutralizer and Mg K_α X-ray source. Spectra were recorded at normal emission using an analyzer pass energy of 40 eV and X-ray power of 225 W. Energy referencing was employed using adventitious carbon and the valence band. Spectra were Shirley background-subtracted and fitted using CasaXPS Version 2.1.9. EXAFS were recorded at room temperature at the Daresbury SRS (Stations 9.3 and 16.5) and ELETTRA synchrotrons (XAFS beamline). Samples were mounted in 2 mm stainless steel washers and where necessary, diluted with BN to achieve absorbances of 1−2. Rh K-edge spectra were recorded between k = 0−14 Å in either transmission for high loading samples or fluorescence for dilute samples, employing a Si(220) monochromator. EXAFS fitting was performed using Excurv98, without Fourier-filtering, and Rh oxidation states calculated from linear combination fitting of normalized XANES spectra to known standards within the ATHENA version 0.8.56 package.[34]

2.3. Carbonylation. Methanol carbonylation was performed in a purpose-built, packed-bed flow microreactor equipped with Brooks 5850TR mass flow controllers and separate online GC (Shimadzu GC-14B) and MS analysis (300 amu MKS Minitorr). Catalysts (5 mg of Rh per charge) were diluted in low surface area Fisher quartz chips, to obtain a constant bed volume of 1 cm^3, and packed into a quartz tube (1 cm i.d.) with silica wool. The reactor tube was linked to the analysis via heated stainless steel lines (70 °C) to prevent condensation of reactants and products. Light-offs were performed at 5 °C min^{-1} from room temperature to 350 °C. MeOH (Fisher 99.5%) was fed via a peristaltic pump at 0.61 cm^3 h^{-1} into a flow of 8 cm^3 min^{-1} CO (Aldrich 99.9%) diluted in 24 cm^3 min^{-1} He carrier gas at 1 bar total pressure. Catalytic data were obtained via online MS, with parallel online GC performed every 10 min to verify all selectivities, yields and mass-balances. GC analysis via a gas-sampling valve utilized a Carboxen1006 Plot column (30 m × 0.53 mm). The following gaseous products were tracked by MS: He (m/z = 4), water (m/z = 18), ethane (m/z = 26), CO (m/z = 28), MeOH (m/z = 32), propane (m/z = 39), DME (m/z = 46), AcOH (m/z = 60), MeOAc (m/z = 74), as well as m/z = 43 which is the major component for both acetyls and propane, representing CH_3CO or C_3H_7 fragments respectively. GC and MS data were corrected for appropriate response factors (obtained using pure standards), to calculate mass balances based on MeOH conversion (which were ∼98% closure), and selectivity to acetyls defined as:

$$\text{Acetyl selectivity \%} = \frac{\{[\text{MeOAc}] + [\text{AcOH}]\}}{\{[\text{MeOAc}] + [\text{AcOH}] + [\text{DME}]\}} \times 100$$

with product concentrations in mmol per hour. Because of the relatively high 1:1 MeOH:CO molar ratio employed in our study, methyl acetate was the dominant acetyl product, with negligible acetic acid formed. Steady state measurements were conducted by heating the catalyst to temperature under He before introducing the CO/MeOH feed under isothermal conditions.

DME carbonylation was also performed on the 1:1 RhXHPW/SiO_2, using an identical catalyst bed and GHSV (1920 h^{-1}) to the MeOH carbonylation experiments. The catalyst was heated to 200 °C before isothermal treatment with a CO/DME/He gas flow for up to 4 h, using DME:CO molar ratios ranging from 1:1 to 1:7.

3. RESULTS AND DISCUSSION

3.1. RhXHPW Synthesis. A range of solution and solid state methods were used to evaluate the structure and stability of the 1:1 RhXHPW materials. Preservation of the parent frameworks was first explored by DRIFTS (Figure 1), which

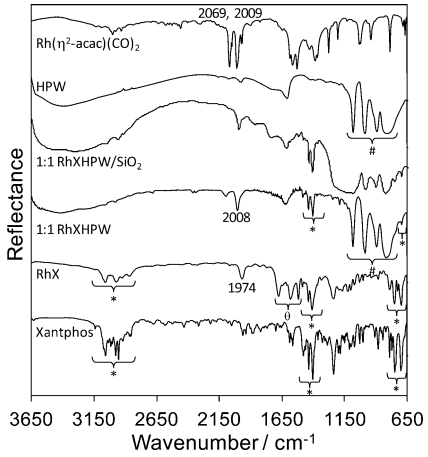

Figure 1. DRIFT spectra of RhX precursor and bulk 1:1 RhXHPW together with representative Rh standards. Characteristic Xantphos (*), HPW (#), and κ^2O-acac bands (θ) are highlighted, together with Rh-CO stretches. Spectra are vertically offset to aid comparison.

showed that the combination of RhX and acidic HPW gave a solid compound with bands at 670, 1400, and 2008 cm^{-1} characteristic of the C−P, C−C, and phenyl/methyl C−C stretching modes of Xantphos, indicating retention of the organic ligand. RhX itself also exhibits a single CO stretching band at 1974 cm^{-1} arising from loss of one CO ligand upon Xantphos complexation with Rh(κ^2O-acac)$(CO)_2$, which in turn originally displayed bands at 2069 and 2009 cm^{-1} due to the symmetric and asymmetric υ_{CO} bands, respectively.[35] This Rh-CO band shifts down to 2008 cm^{-1} in the RhXHPW compound, indicating the electronic structure of Rh is perturbed via interaction with the Keggin anion, likely reflecting protonation and loss of the acac ligand (supported by ^1H NMR see Supporting Information, Figure S3) to yield an ionic $[Rh(CO)(Xantphos)]^+[H_2PW_{12}O_{40}]^-$ compound. The integrity of the phosphotungstate cage within RhXHPW is apparent from the characteristic bands between 700 and 1200 cm^{-1} and overtone at 2100 cm^{-1}.[36] The bulk and surface compositions of RhX and the RhXHPW materials were determined by inductively coupled plasma-optical emissions spectrometry (ICP-OES) and XPS (Table 1 and 2). The P, Rh, and W values were in excellent agreement with the nominal bulk

dx.doi.org/10.1021/cs3000528 | ACS Catal. 2012, 2, 1368−1376

Table 1. Bulk Elemental Analysis and Per Keggin Stoichiometries for RhXHPW-SiO_2[a]

	RhX:HPW ratio							
	0.5:1		1:1		2:1		3:1	
element	wt %	Keggin	wt %	Keggin	wt %	Keggin	wt %	Keggin
C	8.9	35.2	8.5	49.3	14.6	98.5	19.5	143.6
H	1.3	61.0	1.6	109.4	1.5	117.5	1.7	152.4
P	1.6	2.5 (2.5)	1.4	3.0 (3)	2.1	5.5 (5)	2.7	7.8 (7)
Rh	1.0	0.45 (0.5)	1.4	0.96 (1)	2.6	2.0 (2)	3.7	3.1 (3)
W	46.3	12 (12)	31.8	12 (12)	27.2	12 (12)	25.0	12 (12)

[a]Structure 2 predictions in parentheses.

Table 2. RhX and RhXHPW Surface Stoichiometries[a,b]

element	RhX (theory)	RhX (observed)	RhXHPW (theory)	RhXHPW (observed)
C	68 (45)	63 (40)	C	68 (45)
O	23 (4)	42 (42)	O	23 (4)
P	2 (2)	3 (3)	P	2 (2)
Rh	1 (1)	1 (1)	Rh	1 (1)
W		12 (12)	W	

[a]Structure 1 and 2 predictions in parentheses. [b]Calculated from XPS derived atom % content normalized to Rh.

stoichiometries and structure proposed in Scheme 2, with a 1 (Rh):2 (P) ratio observed for RhX, and 1 (Rh):3 (P):12 (W) ratio for RhXHPW. In contrast, the C and O contents deviate significantly from their predicted values, suggesting residual solvent and/or adventitious organic contaminants following attempted solvent removal and sample washing. Attempts to confirm the structure of RhXHPW using single crystal X-ray diffraction were unsuccessful. Despite numerous attempts using a range of methods and solvent combinations no suitable crystals could be obtained. In one instance a crystal of [RhCl(CO)(Xantphos)]·1.5THF was obtained (see Supporting Information) which has presumably been formed from a trace of a chloride-containing impurity in the starting material, or by chloride scavenging from a solvent. A structure of the CH_2Cl_2 solvate of [RhCl(CO)(Xantphos)] has previously been reported.[30]

The oxidation state of Rh within both RhXHPW and RhXHPW/SiO_2 was subsequently probed by XANES and XPS to confirm that the electronic structure of rhodium remained essentially unchanged in accordance with our proposed synthetic route. Figure 2 reveals the XANES spectrum of the Rh(κ^2*O*-acac)$(CO)_2$ precursor is intermediate between representative Rh(0) and Rh(III) standards, consistent with a formally +1 oxidation state, and closely resembles that of the pure and supported RhXHPW samples. As might be anticipated from Scheme 2, sequential exchange of CO for Xantphos and acac for a Keggin anion does not appear to strongly perturb the Rh oxidation state. This observation is supported by high resolution Rh 3d XP spectra (Figure 3a) which reveal that both

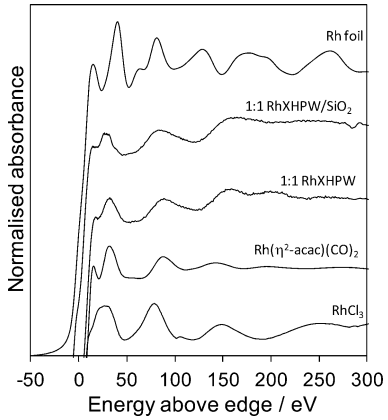

Figure 2. Normalized Rh K-edge XANES of bulk and silica supported 1:1 RhXHPW and representative Rh standards. Spectra are vertically offset to aid comparison.

RhX and RhXHPW exhibit $3d_{5/2}$ binding energies (BEs) consistent with Rh(I) species,[37] although displacement of the acac ligand from the free RhX complex by the noncoordinating, doubly protonated $H_3PW_{12}O_{40}$ anion induces a 0.6 eV shift to higher energy from 308.60 to 309.27 eV which is attibuted to a change in the Madelung potential and final state screening upon embedding the organorhodium species within an ionic framework. A corresponding decrease in the W 4f binding energy of the Keggin unit from 36.8 to 36.3 eV is also observed following complexation with RhX (Figure 3b), consistent with the greater electropositive character of Rh^+ compared to $H_5O_2^+$ and thus greater initial state tungsten charge. Similar shifts have been reported for Cs^+ exchanged heteropoly acids.[38] Around 20% of Keggin units retain characteristics of the parent HPW precursor within the RhXHPW material. Electronic properties of the parent RhXHPW ionic compound were preserved following supporting on silica, with negligible shifts in the binding energies of either the Rh or the dominant W chemical species; the trace unreacted HPW exhibited a 1.5 eV BE decrease on contacting with silica as previously reported.[33] In addition, ^{31}P MAS NMR spectra of RhXHPW and the silica-supported material exhibit resonances for both *coordinated*

Scheme 2. Synthesis and Proposed Structures of RhX (1) and RhXHPW (2) from Rh(κ^2*O*-acac)$(CO)_2$

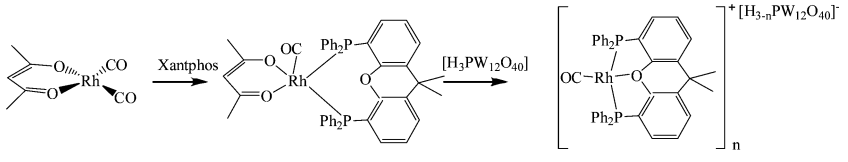

1 2

dx.doi.org/10.1021/cs3000528 | ACS Catal. 2012, 2, 1368−1376

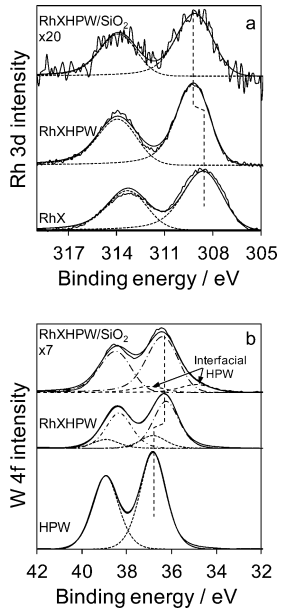

Figure 3. (a) Rh 3d XP spectra of RhX and bulk 1:1 RhXHPW and (b) W 4f XP spectra of 1:1 RhXHPW and bulk HPW. Spectra are vertically offset to aid comparison.

Xantphos ligands and the HPA units (Supporting Information, Figure S4).

The local chemical environment of Rh within RhX and RhXHPW was further probed by EXAFS (Supporting Information, Figure S5), and the resulting fitted radial distribution functions are shown in Figure 4. It is evident

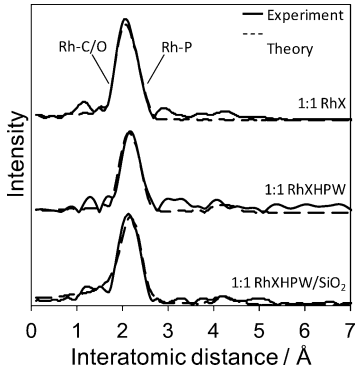

Figure 4. Fitted Rh K-edge EXAFS radial distribution functions of RhX, bulk 1:1 RhXHPW, and 1:1 RhXHPW/SiO_2. Spectra are vertically offset to aid comparison.

from the fitted parameters in Table 3 that the first coordination shells of both RhX and RhXHPW are in good agreement with the structures proposed in Scheme 2, and by van Leeuwen for Rh(κ^2*O*-acac)(CO)(Xantphos) and the analogous RhX^+OTf^- or RhX^+OTf^- variants. Indeed the Rh−P bond lengths of 2.26−2.29 Å, and Rh−O/C distances of 2.05 Å, are very close to those derived from the crystal structure of [Rh(Xantphos)-CO][BF_4]. Incorporation of next nearest neighbor W scatterers (~4 Å) failed to improve the fit, discounting the possibility of a formal covalent Rh−O═W interaction (as observed in related Ru complexes[36]), and supporting the proposed ionic compound in Scheme 2. It is important to note that supporting on silica had minimal influence on the RhXHPW structure, consistent with our previous investigations of phosphotungstic acid adsorption on silica[32,33] which revealed that highly dispersed Keggin units bind via protonation of surface silanols and the formation of a tripod of electrostatic bonds between three interfacial W atoms and the support, while retaining the crystallographic structure and intrinsic reactivity of the parent heteropoly acid. Careful examination of the total first coordination shell intensity reveals a slight attenuation following HPW incorporation, consistent with loss of the acac ligand and the associated reduction in total first shell coordination number from 5 to 4.

Methanol carbonylation is often conducted at elevated temperature, hence the thermal robustness of RhXHPW was assessed by TGA (Supporting Information, Figure S6) which revealed the loss of physisorbed water and water of crystallization at 100 and 200 °C, respectively, and subsequent decomposition of the Xantphos ligand at 400 °C, evidencing the coexistence of intact HPW and Xantphos components within the RhXHPW compound, consistent with the successful synthesis of structure **2**. In-situ stability under reaction conditions is now recognized as a critical feature of any catalytic process, however it is encouraging to note that the residual Xantphos ligand and partially dehydrated ($HPW{\cdot}6H_2O$) Keggin cage impart good thermal stability to RhXHPW up to 400 °C, potentially offering a wide temperature regime for catalytic operation.

3.2. Methanol Carbonylation. The catalytic performance of RhXHPW materials was subsequently investigated toward ambient pressure methanol carbonylation (Figure 5) and benchmarked against pure HPW, which is known to selectively catalyze MeOH condensation to DME above 170 °C,[32] favoring light alkanes at above 300 °C. Under light-off conditions the unsupported HPW performed poorly, with only 30% conversion reached by 280 °C. Despite the bulk 1:1 RhXHPW containing only one-third the number of acid sites present within the reactor charge, it significantly outperformed this HPW benchmark, evidencing a synergy between the organorhodium and the heteropoly acid functions (the RhX precursor is inactive), precisely as hoped. However, the bulk RhXHPW still only delivered 40% conversion at temperatures low enough to minimize MTG chemistry. The limited conversions for both these unsupported systems likely reflects their low surface areas and concomitant poor acid site accessibility,[39] acting in concert with rapid coking of the parent

Table 3. Fitted EXAFS Parameters for RhX, RhXHPW, and 1:1 RhXHPW/SiO_2

sample	CN1 Rh−O[a]	CN2 Rh−O[b]	CN3 Rh−C[c]	CN4 Rh−P[b]	R1/Å Rh−O[a]	R2/Å Rh−O[b]	R3/Å Rh−C[c]	R4/Å Rh−P[b]	σ1 Rh−O[a]	σ2 Rh−O[b]	σ3 Rh−C[c]	σ4 Rh−P[b]	R^2
RhX	2.2		1.2	1.8	2.04		2.05	2.29	0.002		0.002	0.005	21.0
RhXHPW		0.9	1.1	2.4		2.06	2.06	2.27		0.031	0.010	0.009	57.5
RhXHPW/SiO_2		1.3	1.4	2.1		2.05	2.05	2.26		0.002	0.002	0.005	35.7

[a]Atom from acac ligand. [b]Atom from Xantphos ligand. [c]Atom from CO ligand.

dx.doi.org/10.1021/cs3000528 | *ACS Catal.* 2012, 2, 1368−1376

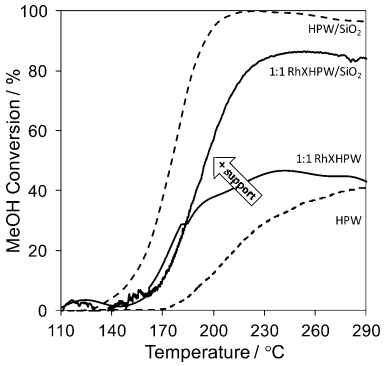

Figure 5. Methanol light-off profiles followed by MS for bulk and silica supported 1:1 RhXHPW and HPW catalysts under standard carbonylation conditions: MeOH:CO = 1:1 molar ratio; GSHV = 2400; reactor charges: 80 mg HPW, 56 mg 1:1 RhXHPW, 311 mg 1:1 RhXHPW/SiO_2 and 250 mg HPW/SiO_2.

HPW. This hypothesis is confirmed by the dramatic decrease in light-off temperature and/or enhanced MeOH conversion seen upon supporting either HPW or RhXHPW on a high area silica support. We have previously shown Davisil silica is particular effective at stabilizing HPW monolayers because of its high surface area (300 m^2 g^{-1}), wide pores and high hydroxyl density which facilities multiple cluster attachment points.[33] In the present case, both silica supported catalysts achieved conversions ≥80% by 200 °C, with the 1:1 RhXHPW/SiO_2 again demonstrating excellent activity despite fewer acid sites than the comparable HPW/SiO_2 sample (further evidence for a synergic interaction between Rh and acid functions). It is important to note that although the HPW/SiO_2 achieved complete methanol conversion by 200 °C, it only produced DME in this low temperature regime with MTG chemistry favored above 300 °C, mirroring the behavior of pure HPW. Dispersion on silica likewise had no effect on the selectivity of RXHPW, which was 50% selective to MeOAc at temperatures below 250 °C, suggesting the support simply imparts enhanced textural properties and does not directly participate in methanol conversion.

Figure 6 shows a typical product distribution for the 1:1 RhXHPW/SiO_2 material. Although methanol condensation is the major low temperature reaction pathway, methyl acetate production commences >150 °C, reaching a maximum at 200 °C corresponding to a peak acetyl selectivity of 56%. DME and acetyl formation remains fairly constant between 200 and 250

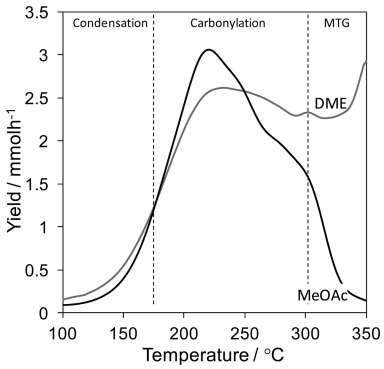

Figure 6. Temperature dependent product distributions followed by MS during methanol light-off over 1:1 RhXHPW/SiO_2. MeOH:CO = 1:1 molar ratio; GSHV = 2400.

°C, above which undesired MTG reactions becomes the dominant process. Dispersing RhXHPW on silica had little influence on the temperature dependent product distributions, confirming both catalysts operated via a common reaction mechanism, and the greater reactivity of RhXHPW/SiO_2 over RhXHPW seen in Figure 5 is indeed associated with a higher density of similar active sites. The HPW-only materials did not catalyze carbonylation chemistry, and were only active toward methanol condensation over the same temperature regime. In contrast to "$RhW_{12}PO_{40}/SiO_2$" catalysts prepared via ion-exchange of HPW with a Rh^{3+} precursor,[4] our ionic Rh 1:1 RhXHPW/SiO_2 catalyst also exhibits good activity toward DME carbonylation (and at a higher GHSV), achieving 59% conversion using a 1:7 DME:CO mix at 200 °C over 4 h (Figure 7), with 55% converted to acetyls and only 4% to

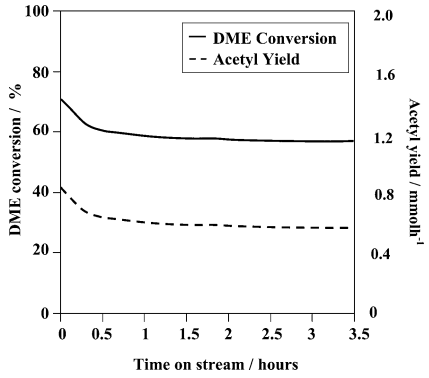

Figure 7. DME conversion and acetyl yield followed by MS of 1:1 RhXHPW-SiO_2 during continuous operation at 200 °C during DME carbonylation (DME:CO = 1:7).

MeOH. Despite the expected drop in conversion with increasing DME concentration, the methyl acetate to methanol product ratio remained >9:1. We should note that despite the mild (atmospheric pressure) reaction conditions, our absolute rate of DME carbonylation to methyl acetate of 0.45 μmol g_{cat}^{-1} s^{-1} is identical to the best reported for Rh/Cs-HPW solid catalysts operating under 10 bar CO and similar flow rates,[20] wherein a bifunctional mechanism, involving CO adsorption at the Rh center and DME activation at Brönsted acid sites, is proposed.[40]

3.3. Catalyst Deactivation. The stability of the 1:1 RhXHPW/SiO_2 catalyst was subsequently assessed by monitoring its time-dependent reactivity at both 200 °C (where peak acetyl production occurs during light-off) and at 250 °C (on the threshold for MTG chemistry). Figure 8 shows the evolving MeOH conversion and acetyl selectivity during the first 2 h on-stream. At both temperatures, rapid initial deactivation occurs over the first 15 min of reaction; however, this is much more severe at 250 °C, for which MeOH conversion falls by 40%, compared with a drop of only 13% at the lower temperature. The steady state activity is also better at 200 °C, and in longer test runs 25% methanol conversion is maintained in excess of 5 h. Similar temperature-dependent deactivation is reported during methanol carbonylation over ion-exchanged Rh heteropoly acids.[4] Our acetyl selectivity mirrors these changes, decreasing precipitously at 250 °C from 66% to only 20% within the same period, with a much smaller decrease observed at 200 °C for which our 1:1 RhXHPW/SiO_2 catalyst remains almost 50% selective to methyl acetate for many hours. There are three distinct explanations for this deactivation: loss of CO

dx.doi.org/10.1021/cs3000528 | ACS Catal. 2012, 2, 1368–1376

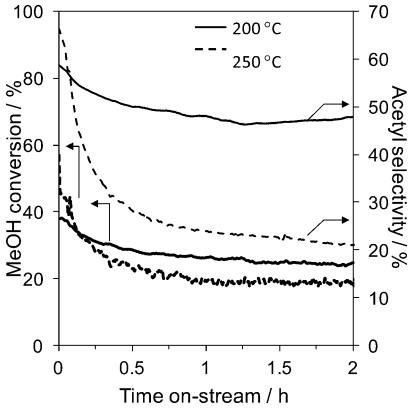

Figure 8. Methanol conversion and acetyl selectivity followed by MS of 1:1 RhXHPW/SiO_2 during continuous operation at 200 and 250 °C under standard carbonylation conditions.

binding through decomposition of the cationic Rh complex; loss of acidity from the HPW component; or morphological changes resulting in a lower surface area or accessibility of both active centers. We will consider each in turn.

Thermal analysis indicates the RhX complex and RhXHPW ionic compound are stable to 300 °C under helium. However, the reducing environment employed in our reactor tests could facilitate the formation of rhodium metal, and associated loss of the positive synergic interaction with HPW anions, which would be particularly detrimental to acetyl selectivity more so than conversion. In-situ Rh K-edge XANES of the 1:1 RhXHPW/SiO_2 catalyst were therefore acquired as a function of time under a highly reducing CO/He flow at 250 °C. The Rh(I) content, derived by least-squares fitting of the normalized XANES to Rh metal, Rh(κ^2*O*-acac)$(CO)_2$ and $RhCl_3$ standards, shows a steep fall during the first 15 min of reaction from ∼75 to 55%, mirroring the falling acetyl yield (Figure 9). Hence, the

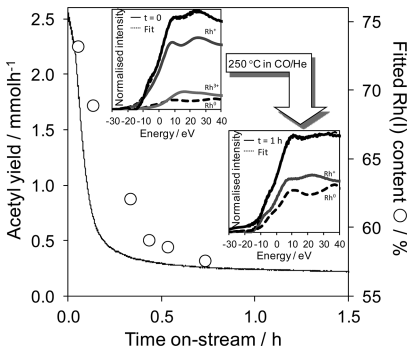

Figure 9. Correlation between catalytic deactivation of 1:1 RhXHPW/SiO_2 catalyst during methanol carbonylation followed by MS under standard conditions at 250 °C and loss of Rh(I) determined by in situ XANES under flowing 25% CO/He mixture at 250 °C. Inset shows least-squares fitted Rh K-edge XANES of fresh and spent 1:1 RhXHPW/SiO_2 to Rh foil, Rh Cl_3, and Rh(κ^2*O*-acac)$(CO)_2$ standards.

$[Rh(CO)(Xantphos)]^+$ component appears readily reducible, with barely half of the Rh remaining ligated after 1 h at at 250 °C. Although this reduction is disappointing from an application perspective, we should note that our RhXHPW/SiO_2 catalyst is much more robust than simpler $Rh(OAc)_2$ or $RhCl_3$ complexes, which are fully reduced over this time scale under the same experiment protocol.[41] This close temporal correspondence between oxidation state and reactivity strongly implicates Rh reduction in the isothermal deactivation apparent in Figure 8.

As noted above, although Rh decomplexation would disfavor selective carbonylation chemistry, it is not obvious that it should affect the intrinsic acidity, and therefore activity, of the HPW component. The parallel drop in MeOH conversion with selectivity therefore suggests rhodium reduction is accompanied by the loss of acid sites, possibly because of coking or dehydration. The latter may occur via hydrolysis of the desired methyl acetate product to acetic acid and methanol. To study whether product self-poisoning was involved in deactivation of the 1:1 RhXHPW/SiO_2 catalyst, a fresh sample was pretreated with MeOAc at 200 °C for 20 min prior to exposure to the standard MeOH/CO carbonylation mixture. Figure 10

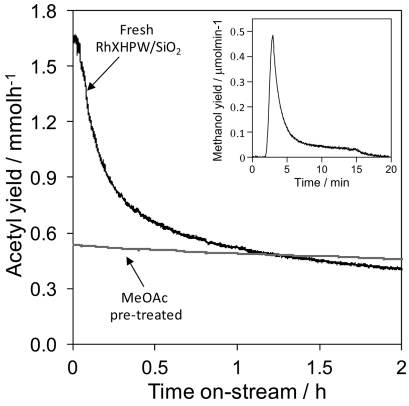

Figure 10. Effect of MeOAc pretreatment on acetyl yield of 1:1 RhXHPW/SiO_2 during methanol carbonylation followed by MS under standard conditions at 200 °C. Pretreatment conditions: 7 mmol h^{-1} MeOAc in 32 mL min^{-1} He at 200 °C for 20 min. Inset shows yield of reactively formed MeOH arising from acetyl hydrolysis during pretreatment.

compares the resulting carbonylation performance with that for a fresh catalyst simply held at reaction temperature under He for the same period. Under standard conditions the acetyl yield decays from ∼2 mmol h^{-1} (i.e., 400 mmol h^{-1} g_{Rh}^{-1}) to a plateau of 0.55 mmol h^{-1}; however, the MeOAc pretreatment completely suppresses this initial high activity phase, apparently transforming the 1:1 RhXHPW/SiO_2 into the same low activity state usually only attained after 2 h reaction. Since this MeOAc-induced deactivation could reflect either coking or the loss of water of crystallization from the vicinity of HPW Keggin units (and therefore acidity) because of hydrolysis, the gas phase methanol concentration was closely monitored during acetate introduction. The inset to Figure 10 clearly shows MeOAc triggers a rapid burst of reactively formed methanol, implicating catalyst dehydration and not coking as a contributor to the deactivation seen in Figure 8. Indeed, the integrated yield of this MeOH spike is 0.12 mmol, close to the theoretical maximum of 0.17 mmol of H_2O molecules available within the catalyst charge, suggesting that high local acetyl concentrations could destroy RhXHPW/SiO_2 solid acidity under reaction conditions. This hypothesis is supported by the result of cofeeding 5 mol % H_2O during our standard 200 °C isothermal carbonylation experiment over RhXHPW/SiO_2. Figure 11 reveals that water addition triples initial acetyl production, and slows the rate of deactivation, conferring a 4-fold enhancement on the steady acetyl yield. However, the precise origin for this promotion has not yet been established, since

dx.doi.org/10.1021/cs3000528 | *ACS Catal.* 2012, 2, 1368−1376

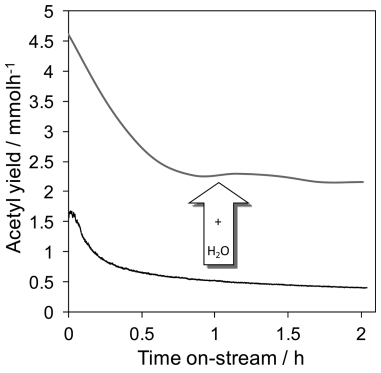

Figure 11. Effect of co-fed H_2O on acetyl yield of 1:1 RhXHPW/SiO_2 during methanol carbonylation followed by MS under standard conditions at 200 °C. MeOH:CO:H_2O = 1:1:0.5 molar ratio.

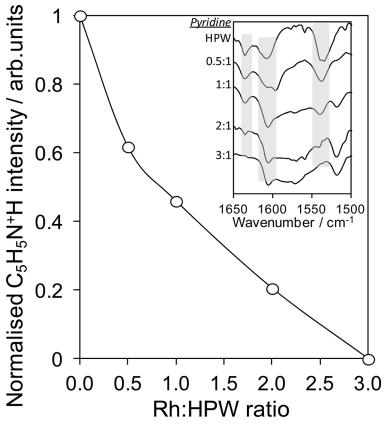

Figure 12. Influence of Rh content on DRIFT spectra-derived pyridinium ion intensity at 1540 cm^{-1} for 1:1 RhXHPW/SiO_2; pyridinium signals have been normalized relative to the 3 protons expected for the parent $H_3PW_{12}O_{40}$. Inset shows associated DRIFT spectra with principal pyridium ion bands highlighted. Spectra are vertically offset to aid comparison.

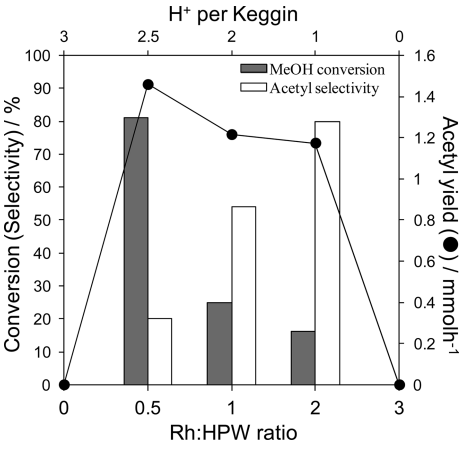

Figure 13. Influence of Rh/H^+ content on steady state methanol conversion, acetyl selectivity and acetyl yield of RhXHPW/SiO_2 followed by MS during methanol carbonylation at 200 °C. The total amount of Rh was kept constant at 5 mg for each catalyst. Acetyl yield is the average over 5 h reaction.

water also participates in competing reactions operating during methanol carbonylation (Scheme 1); for example, H_2O addition may shift the MeOH condensation equilibria away from DME, thus increasing overall selectivity to MeOAc.

Porosimetry on fresh and spent catalysts showed no evidence for morphology changes under reaction conditions, with the surface area only exhibiting a marginal drop from 115 $m^2\ g^{-1}$ to 102 $m^2\ g^{-1}$ postreaction, and the pore volume remaining constant at 0.3 cm^{-3} after 5 h reaction at 200 °C. We can thus discount, for example, crystallization of the silica support or pore blocking by coke as responsible for the observed deactivation.

3.4. Catalyst Optimization. The ionic character of our bifunctional RhXHPW catalysts subsequently enabled us to explore the impact of Rh:HPW ratio, and thus notionally CO binding capacity versus solid acidity, on net carbonylation performance. Additional RhXHPW/SiO_2 samples with Rh:HPW ratios spanning 0.5:1, 2:1, and 3:1 (Table 1) were prepared from the same 50 wt % HPW/SiO_2 precursor used to synthesize the 1:1 Rh:HPW material, and their acidic and reactive properties screened. Elemental analysis showed the Rh:W:P stoichiometry could be carefully tuned as desired, and the mass loss of water determined from TGA (Supporting Information, Figure S7, Table S1) was consistent with a transition from the triply protonated Rh-free precursor to a fully deprotonated 3:1 RhXHPW/SiO_2 (confirming the exchange of one proton for each organorhodium cation, and thus Rh^+ oxidation state). The sequential exchange of Keggin protons should correlate with a progressive loss in RhXHPW/SiO_2 acidity, and indeed titration by pyridine (Supporting Information, Figure S8) supports this; the DRIFT spectral pyridinium ion intensity at 1540 cm^{-1}, characteristic of Brönsted surface acid sites (Supporting Information, Table S2), decreases monotonically with increasing Rh content (Figure 12), with the 3:1 RhXHPW/SiO_2 losing all Brönsted acidity.

The corresponding reactivity of this RhXHPW/SiO_2 series was assessed during 5 h isothermal carbonylation at 200 °C (Supporting Information, Figures S9–10), the optimal temperature for the 1:1 Rh:HPW/SiO_2 catalyst. Figure 13 shows the resulting MeOH conversion, and acetyl selectivity/yield is strongly influenced by the balance of catalyst components. Rh addition enhances acetyl selectivity, as anticipated if the organorhodium complex provides sites for CO activation, at the expense of acid sites required for methanol activation. This balance between the CO affinity and solid acidity of RhXHPW/SiO_2 produces a volcano dependence on rhodium concentration, with a maximum steady state acetyl yield of 1.5 mmol h^{-1} for Rh:HPW = 0.5:1. Since the peak acetyl yield occurs at a low level of Rh exchange it is likely that carbonylation is limited by Me^+ availability, which in turn may reflect rapid Me^+ consumption via the competing DME condensation pathway. An alternative possibility is that DME itself plays a role in the carbonylation reaction, with low Rh contents (more acid sites) maximizing DME formation via condensation, with secondary DME carbonylation responsible for the final methyl acetate product (our RhXHPW/SiO_2 catalysts being notably active for this latter step).

4. CONCLUSIONS

Sequential reaction between the widely available Rh(κ^2*O*-acac)$(CO)_2$ precursor, tridentate Xantphos ligand, and silica-supported phosphotungstic acid affords a simple route to a new family of robust, ionic $[Rh(CO)(Xantphos)]^+_n[H_{3-n}PW_{12}O_{40}]^{n-}/SiO_2$ heterogeneous catalysts suitable for vapor phase methanol carbonylation under mild reaction conditions

dx.doi.org/10.1021/cs3000528 | ACS Catal. 2012, 2, 1368–1376

(1 bar and 200 °C). Their good rates of methyl acetate production, equating to an optimum space-time yield of 350 g kg_{cat}^{-1} h^{-1}, reflect the synergy between the (i) solid acid character of the parent $H_3PW_{12}O_{40}$ necessary for low temperature Me^+ generation, (ii) CO affinity of the stable $[Rh(CO)(Xantphos)]^+$ complex, and (iii) high active site density afforded by dispersed HPW monolayers over Davisil silica. Catalyst deactivation remains problematic, especially at high temperatures which drive Rh reduction to the metallic state, and simultaneous loss of water and solid acidity from the Keggin framework which can be partially prevented by water addition to the reactant stream. Catalyst performance is sensitive to the degree of proton exchange, reflecting an inverse correlation between selectivity to acetyls (favored by Rh) versus MeOH conversion (favored by HPW), with the optimum methyl acetate yield achieved for Rh:HPW = 0.5.

■ ASSOCIATED CONTENT

Supporting Information

Additional catalyst characterization and MeOH carbonylation reaction profiles for different Rh:HPW ratios, and the Crystallographic Information File (CIF) for [RhCl(CO)-(Xantphos)]·1.5THF. This material is available free of charge via the Internet at http://pubs.acs.org.

■ AUTHOR INFORMATION

Corresponding Author

*E-mail: leeaf@cardiff.ac.uk (A.F.L.), jason.lynam@york.ac.uk (J.M.L.), wilsonk5@cardiff.ac.uk (K.W.). Phone: 44 (0)2920 874778.

Funding

L.D.D. thanks BP Chemicals Ltd and the EPSRC for the award of a Ph.D. studentship, and A.F.L. thanks the EPSRC for the award of a Leadership Fellowship (EP/G007594/2).

Notes

The authors declare no competing financial interest.

■ ACKNOWLEDGMENTS

We thank Dr. Adrian Whitwood for the crystal structure of [RhCl(CO)(Xantphos)]·1.5THF.

■ REFERENCES

(1) Haynes, A.; Maitlis, P. M.; Morris, G. E.; Sunley, G. J.; Adams, H.; Badger, P. W.; Bowers, C. M.; Cook, D. B.; Elliott, P. I. P.; Ghaffar, T.; Green, H.; Griffin, T. R.; Payne, M.; Pearson, J. M.; Taylor, M. J.; Vickers, P. W.; Watt, R. J. *J. Am. Chem. Soc.* **2004**, *126*, 2847−2861.

(2) Haynes, A. In *Advances in Catalysis*; Gates, B. C., Helmut, K., Eds.; Academic Press: New York, 2010; Vol. *53*, pp 1−45.

(3) Maitlis, P. M.; Haynes, A.; Sunley, G. J.; Howard, M. J. *J. Chem. Soc., Dalton Trans.* **1996**, 2187−2196.

(4) Wegman, R. W. U.S. Patent US5330955, Union Carbide Chem Plastic, 1994.

(5) Blasco, T.; Boronat, M.; Concepcion, P.; Corma, A.; Law, D.; Vidal-Moya, J. A. *Angew. Chem., Int. Ed.* **2007**, *46*, 3938−3941.

(6) Ditzel, E. J.; Law, D. J.; Morris, G. E.; Roberts, M. S.; Schunk, S. A.; Smit, M.; Sunley, J. G. WO/2009/077745, BP Chemicals Ltd, 2009.

(7) Hedrick, S. A.; Chuang, S. S. C.; Pant, A.; Dastidar, A. G. *Catal. Today* **2000**, *55*, 247−257.

(8) Chuang, S. S. C.; Stevens, R. W.; Khatri, R. *Top. Catal.* **2005**, *32*, 225−232.

(9) Howard, M. J.; Jones, M. D.; Roberts, M. S.; Taylor, S. A. *Catal. Today* **1993**, *18*, 325−354.

(10) Bhasin, M. M.; Bartley, W. J.; Ellgen, P. C.; Wilson, T. P. *J. Catal.* **1978**, *54*, 120−128.

(11) Nakajo, T.; Sano, K.; Matsuhira, S.; Arakawa, H. *J. Chem. Soc., Chem. Commun.* **1987**, 647−649.

(12) Fouad, N. E.; Mohamed, M. A.; Zaki, M. I.; Knozinger, H. *J. Anal. Appl. Pyrolysis* **2000**, *53*, 185−193.

(13) Shinoda, S.; Yamakawa, T. *J. Chem. Soc., Chem. Commun.* **1990**, 1511−1512.

(14) Ellis, B.; Howard, M. J.; Joyner, R. W.; Reddy, K. N.; Padley, M. B.; Smith, W. J. Heterogeneous catalysts for the direct, halide-free carbonylation of methanol. In *Proceedings of the 11th International Congress on Catalysis - 40th Anniversary, Pts A and B*; Hightower, J. W., Delgass, W. N., Iglesia, E., Bell, A. T., Eds.; Elsevier Science Publ B V: Amsterdam, The Netherlands, 1996; Vol. *101*, pp 771−779.

(15) Fujimoto, K.; Shikada, T.; Omata, K.; Tominaga, H. *Chem. Lett.* **1984**, 2047−2050.

(16) Smith, W. J., U.S. Patent US 5420345, BP Chemicals Ltd, 1995.

(17) Cheung, P.; Bhan, A.; Sunley, G. J.; Iglesia, E. *Angew. Chem., Int. Ed.* **2006**, *45*, 1617−1620.

(18) Ormsby, G.; Hargreaves, J. S. J.; Ditzel, E. J. *Catal. Commun.* **2009**, *10*, 1292−1295.

(19) Wegman, R. W. *J. Chem. Soc., Chem. Commun.* **1994**, 947−948.

(20) Volkova, G. G.; Plyasova, L. M.; Salanov, A. N.; Kustova, G. N.; Yurieva, T. M.; Likholobov, V. A. *Catal. Lett.* **2002**, *80*, 175−179.

(21) Ali, B.; Tijani, J.; Fettouhi, M. *J. Mol. Catal. A: Chem.* **2006**, *250*, 153−162.

(22) Kozhevnikov, I. V. *Chem. Rev.* **1998**, *98*, 171−198.

(23) Mizuno, N.; Misono, M. *Chem. Rev.* **1998**, *98*, 199−217.

(24) Hill, C. L. *J. Mol. Catal. A: Chem.* **2007**, *262*, 2−6.

(25) Li, G. X.; Ding, Y.; Wang, J. M.; Wang, X. L.; Suo, J. S. *J. Mol. Catal. A: Chem.* **2007**, *262*, 67−76.

(26) Luzgin, M. V.; Kazantsev, M. S.; Wang, W.; Stepanov, A. G. *J. Phys. Chem. C* **2009**, *113*, 19639−19644.

(27) Sandee, A. J.; van der Veen, L. A.; Reek, J. N. H.; Kamer, P. C. J.; Lutz, M.; Spek, A. L.; van Leeuwen, P. W. N. M. *Angew. Chem., Int. Ed.* **1999**, *38*, 3231−3235.

(28) van Leeuwen, P. W. N. M.; Sandee, A. J.; Reek, J. N. H.; Kamer, P. C. J. *J. Mol. Catal. A: Chem.* **2002**, *182*, 107−123.

(29) Gaemers, S.; Sunley, G. J. WO/2004/101488, BP Chemicals Ltd, 2004.

(30) Williams, G. L.; Parks, C. M.; Smith, C. R.; Adams, H.; Haynes, A.; Meijer, A. J. H. M.; Sunley, G. J.; Gaemers, S. *Organometallics* **2011**, *30*, 6166−6179.

(31) Gaemers, S.; Law, D. J.Sunley, J. G., EP11250728.0 to BP Chemicals Limited.

(32) Newman, A. D.; Lee, A. F.; Wilson, K.; Young, N. A. *Catal. Lett.* **2005**, *102*, 45−50.

(33) Newman, A. D.; Brown, D. R.; Siril, P.; Lee, A. F.; Wilson, K. *Phys. Chem. Chem. Phys.* **2006**, *8*, 2893−2902.

(34) Ravel, B.; Newville, M. *Phys. Scr.* **2005**, *T115*, 1007−1010.

(35) Bonati, F.; Wilkinson, G. *J. Chem. Soc.* **1964**, 3156−3160.

(36) Dingwall, L. D.; Corcoran, C. M.; Lee, A. F.; Olivi, L.; Lynam, J. M.; Wilson, K. *Catal. Commun.* **2008**, *10*, 53−56.

(37) Vantblik, H. F. J.; Vanzon, J. B. A. D.; Huizinga, T.; Vis, J. C.; Koningsberger, D. C.; Prins, R. *J. Am. Chem. Soc.* **1985**, *107*, 3139−3147.

(38) Narasimharao, K.; Brown, D. R.; Lee, A. F.; Newman, A. D.; Siril, P. F.; Tavener, S. J.; Wilson, K. *J. Catal.* **2007**, *248*, 226−234.

(39) Kozhevnikov, I. V. *Catal. Rev.—Sci. Eng.* **1995**, *37*, 311−352.

(40) Luzgin, M. V.; Kazantsev, M. S.; Volkova, G. G.; Wang, W.; Stepanov, A. G. *J. Catal.* **2011**, *277*, 72−79.

(41) Newman, A. D. Structure and reactivity of rhodium promoted heteropoly acid catalysts. Ph.D. Thesis, University of York, York, U.K. 2007.